Bioactive Materials 50 (2025) 382–395

Contents lists available at ScienceDirect

Bioactive Materials

journal homepage: www.keaipublishing.com/en/journals/bioactive-materials

Macrophage response to fibrin structure mediated by Tgm2-dependent mitochondrial mechanosensing

Bicong Gao [a,1], Haifeng Ni [b,1], Junhong Lai [a,1], Ning Gao [a], Xinxin Luo [b], Ying Wang [a], Yani Chen [a], Jiaying Zhao [a], Zhou Yu [a], Jing Zhang [b,*], Wenjin Cai [a,**], Guoli Yang [a,***]

[a] Stomatology Hospital, School of Stomatology, Zhejiang University School of Medicine, Zhejiang Provincial Clinical Research Center for Oral Diseases, Key Laboratory of Oral Biomedical Research of Zhejiang Province, Cancer Center of Zhejiang University, Engineering Research Center of Oral Biomaterials and Devices of Zhejiang Province, Hangzhou, 310000, China

[b] Zhejiang Key Laboratory of Plastic Modification and Processing Technology, College of Materials Science & Engineering, Zhejiang University of Technology, Hangzhou, 310014, China

ARTICLE INFO

Keywords:
Biomaterial recognition
Foreign body response
Mitochondrion
Mechanotransduction
Transglutaminase

ABSTRACT

Following an injury at the implantation position, blood-material interactions form a fibrin architecture, which serves as the initial activator of foreign body response (FBR). However, there is limited knowledge regarding how the topography of fibrin architectures regulates macrophage behavior in mitigating FBR. Mechanical cues of the microenvironment have been reported to shape immune cell functions. Here, we investigated macrophage mechanobiology at the organelle level by constructing heterogeneous fibrin networks. Based on findings *in vivo*, we demonstrated that adhesion-mediated differentiation of mitochondrial function modulated macrophage polarization. The finite activation of integrin signaling upregulated transglutaminase 2 (Tgm2) in a trans-manner, augments PGC1α-mediated mitochondrial biogenesis. Our study highlighted the previously overlooked spatial structures of host proteins adsorbed on material surfaces, advocating for a paradigm shift in material design strategies, from focusing solely on physical properties to considering the modification of host proteins.

1. Introduction

Implantable medical devices provide undisputable benefits to patients with organ dysfunction. However, the foreign body response (FBR), an immune response by the host's innate immune system, remains a major challenge. Adverse outcomes of FBR include aseptic loosening in joint prostheses [1,2], chronic pain and misalignment of breast implants [3,4], and encapsulation of cardiovascular implants [5], often compromising the intended purpose of biomaterial implantation. Addressing FBR has therefore been a longstanding challenge for all biomaterial development.

Among the various innate immune cells, macrophages have been considered the main force in determining the success of tissue repair during FBR [6]. In the initial phase of FBR, the adsorption of host proteins on the surface of implanted materials, creates localized mechanical microenvironments that critically regulate macrophage responses [7,8]. Recruited macrophages polarize into either the M1 pro-inflammatory phenotype or the M2 pro-healing phenotype, initiating the cascade of FBR. Traditional strategies to thwart FBR have focused on preventing protein adsorption through modifications to the charge or wettability of material surfaces, such as anti-fouling hydrogels [9–12] and hydrophilic surface coatings [13–15]. However, these strategies are inherently limited due to the inevitable and continuous exposure to body fluid. A shift in the research paradigm is required to understand how the mechanomorphology of adsorbed proteins on biomaterial surfaces influences macrophage mechanobiology, moving from strategies of avoidance to those of constructive engagement.

The fibrin architecture, typically formed on the biomaterial surface through blood-material interactions (i.e., the Vroman effect) [16], serves as a scaffold that macrophages infiltrate [17,18].

Peer review under the responsibility of editorial board of Bioactive Materials.
* Corresponding author.
** Corresponding author.
*** Corresponding author.
E-mail addresses: zhangjing@zjut.edu.cn (J. Zhang), wenjincai0226@zju.edu.cn (W. Cai), guo_li1214@zju.edu.cn (G. Yang).
[1] These authors contributed equally to this work.

https://doi.org/10.1016/j.bioactmat.2025.04.022
Received 20 February 2025; Received in revised form 17 April 2025; Accepted 17 April 2025

Fibrinogen-deficient mice, which fail to form fibrin polymers, exhibit a dramatic reduction in macrophage fusion and fibrous capsule formation, identifying fibrin networks as a critical biology substrate driving the development of the FBR [19]. Containing the binding sites of integrin, fibrin networks transmit biomechanical signals that mediate macrophage inflammation and innate immunity via cell-extracellular matrix (ECM) interaction in the injury microenvironment [20]. Recent findings suggest that thinner fibrin networks with reduced contact area inhibit macrophage inflammation [21], highlighting the potential for tailoring fibrin network mechanics as a novel strategy to address FBR.

Despite recent advancements, the mechanobiology of macrophages remains poorly understood, with most research concentrating on substrate stiffness [22]. Macrophages sense substrate stiffness via adhesion-dependent mechanosensing, which modulates inflammatory responses through cytomembrane deformation and activation of yes-associated protein (YAP) [23,24]. Mechanosensitive ion channels, such as Piezo-type mechanosensitive ion channel component 1 (PIEZO1) and transient receptor potential vanilloid 4 (TRPV4), are also implicated in regulating macrophage responses to stiffness [25,26]. Notably, mitochondria, a central signaling hub, have emerged its

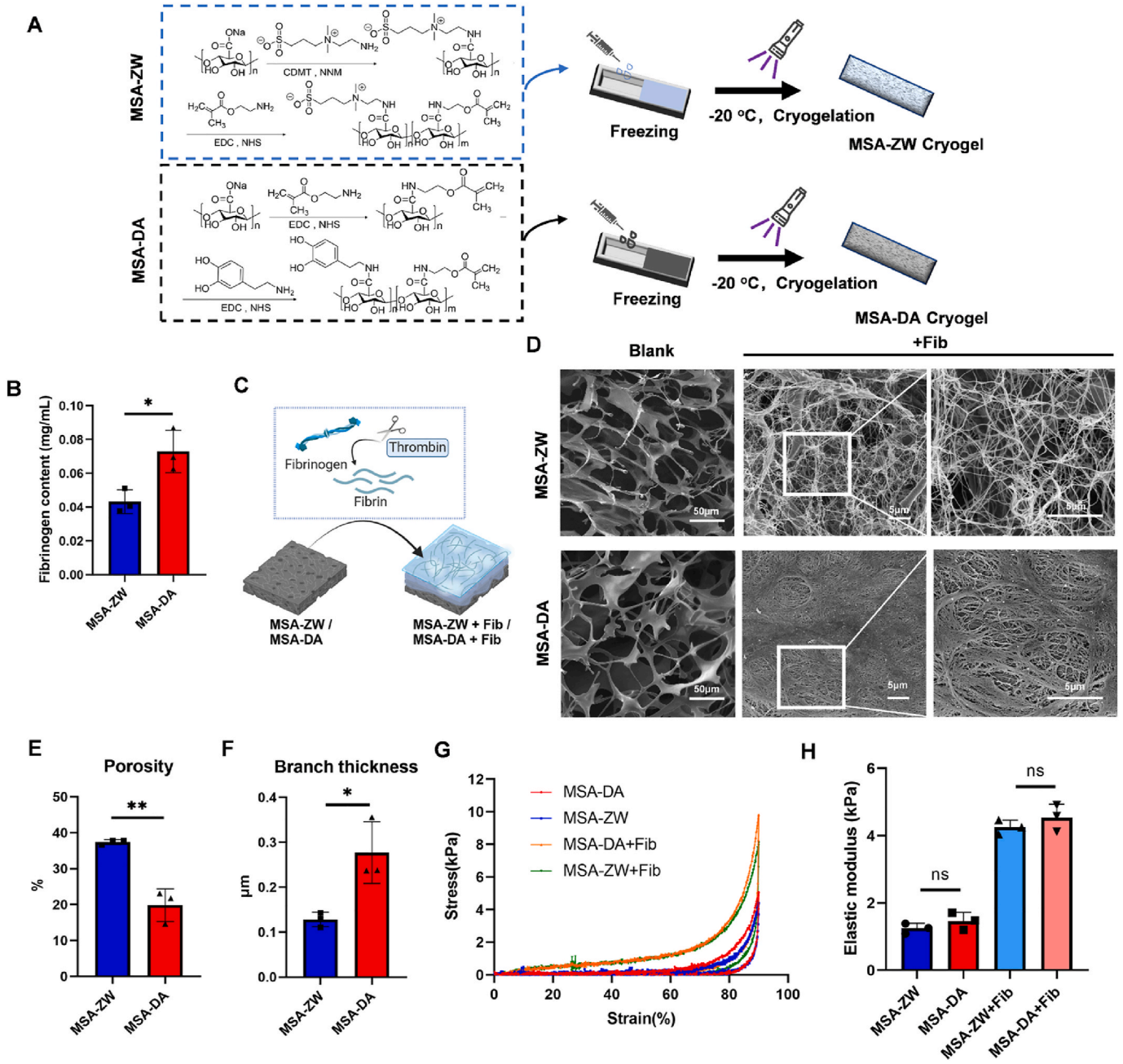

Fig. 1. Macroporous hydrogels with varying protein absorption capacities resulted in distinct fibrin network structures. (A) Synthesis process of MSA-ZW and MSA-DA. (B) The fibrinogen content reflecting fibrinogen absorption MSA-ZW and MSA-DA (n = 3, two-tailed Student's t-test, $^{*}P < 0.05$). (C) Schematic diagram of fibrin network formation. MSA-ZW and MAS-DA were incubated with fibrinogen and thrombin, leading to the cleavage and subsequent rearrangement of fibrinogen into fibrin networks. (D–F) Representative images of SEM images and quantification of fibrin network. (E) MSA-ZW and MSA-DA without fibrin network were labeled as "blank." Scale bar, 50 μm. The presence of fibrin networks on MSA-ZW and MSA-DA was labeled as "+Fib." Scale bar, 5 μm. (E) Quantification of the porosity (n = 3, two-tailed Student's t-test, $^{**}P < 0.01$). (F) Quantification of the branch thicknesses (n = 3, two-tailed Student's t-test, $^{*}P < 0.05$). (G) Compression Curve of macroporou hydrogels with or without fibrin network. (H) Elastic modulus of macroporou hydrogels with or without fibrin network (n = 3, two-tailed Student's t-test, ns, no significance).

mechanosensitive properties recently. Cells detect ECM stiffness through integrin-mediated adhesion, which regulates mitochondrial dynamics to coordinate cell proliferation, differentiation, and survival [27,28]. Furthermore, fluid shear stress sensed by primary cilia has been reported to induce mitochondrial biogenesis in kidney epithelial cells [29]. Nevertheless, mitochondria mechanotransduction has not yet been established in the context of macrophage, overlooking the critical interplay between mitochondrial function and macrophage biology [30].

Here, we developed a model system to investigate the effects of different fibrin network structures on macrophages by modifying methacrylated sodium alginate with zwitterionic (sulfobetaine) or dopamine groups (referred to as MSA-ZW and MSA-DA, respectively) [10,31]. We found that these materials generated distinct fibrin networks that modulate macrophage mitochondrial mechanosensing in an integrin-dependent manner, influencing early inflammatory responses in FBR. Furthermore, we identified a novel mechanical responsiveness of transglutaminase 2 (Tgm2), a versatile enzyme, in regulating mitochondrial biogenesis. This study not only introduces a research paradigm for understanding biomaterial-host protein interactions but also advances knowledge of macrophage mechanobiology, offering a new strategy for the design of future biomaterials.

2. Results

2.1. Heterogeneity of hydrogel protein adsorption capacity resulted in distinct fibrin architecture and FBR

The FBR is promptly triggered upon implant contact with blood, leading to the swift adsorption of host proteins. This initial matrix layer is significantly influenced by the physiochemical properties of the implant materials and acts as a "fingerprint" recognized by the host innate immune system [7]. We hypothesized that the spatial structure of host proteins shapes the preemptive immunity, therefore influencing the long-term outcomes of tissue healing. To verify this hypothesis, we developed two microporous hydrogels with distinct surface modifications: dopamine-modified MSA-DA and zwitterionic SB-modified MSA-ZW (Fig. 1A). Zwitterionic modification is known to provide high surface hydration, which resists protein adsorption, while dopamine modification enhances the adhesive properties of alginate. 1H nuclear magnetic resonance (1H NMR) spectroscopy confirmed the successful incorporation of dopamine functional groups and zwitterionic SB groups (Fig. S1A). MSA-ZW and MSA-DA exhibited excellent shapeability and rapidly reached the equilibrium swelling state in 1min (Fig. S1B and C). Notably, blood clotting test demonstrated that MSA-DA stimulated blood coagulation more effectively than MSA-ZW (Fig. S1D), signifying that surface chemical modifications substantially altered the behavior of protein adsorption. Considering fibrin(ogen) is a key biological substrate driving FBR development [19,32], we incubated fibrinogen with the hydrogels and observed that MSA-DA absorbed more fibrinogen than MSA-ZW (Fig. 1B). To simulate and analyze protein network formation during FBR *in vitro*, fibrinogen was cleaved by thrombin and allowed to form networks on the hydrogel surfaces (Fig. 1C). This process mimics the initial interaction between host proteins and the material surfaces, akin to the Vroman effect [16]. As our expectation, fibrin networks formed on MSA-ZW exhibited a loose, porous structure, whereas those on MSA-DA were denser (Fig. 1D). The assessment of fibrin network porosity and branch thickness confirmed that the MSA-DA network had lower porosity and more substantial, densely aggregated branches compared to MSA-ZW (Fig. 1E and F). In addition, the decoration level of dopamine and zwitterionic SB can be controlled through the substrate's charge rate. As the degradation rate of adhesive properties increases, the fibrin network becomes denser (Fig. S1E). Since materials stiffness is a proverbial regulator of FBR [33,34], we measured the mechanical strength of hydrogels. The result showed that MSA-ZW and MSA-DA exhibited similar elastic moduli, whether incubated with fibrinogen or not (Fig. 1G and H).

To evaluate the FBR mediated by the two macroporous hydrogels, they were implanted into the distal femur defect and quadriceps femoris muscle of mice. After surgery, the samples were collected at 1 week, 2 weeks, and 4 weeks post-implantation for histopathological analysis (Fig. 2A). Micro-CT analysis of the femur displayed that the defect size increased over time due to the material occupying the space. In contrast, MSA-ZW implantation induced a slower enlargement of the defect, with the defect size significantly smaller in the MSA-DA group compared to MSA-DA at 2 and 4 weeks post-implantation (Fig. 2B and C). Hematoxylin & Eosin (H&E) staining and Masson's trichrome staining were performed on harvested muscles. Residual hydrogels, loaded with various cells and extracellular matrix (ECM), were observed in the quadriceps femoris muscles. The image showed that fibrosis appeared at 2 weeks, and the thickness of fibrous capsules in the FBR increased in the MSA-DA group (Fig. 2D). Notably, collagen fibers that inserted into muscles were significantly reduced in the MSA-ZW group (Fig. 2E). Taken together, the differences in hydrogel adhesion properties induced markedly distinct fibrin architecture and host FBR, although the underlaying relationship remains elusive.

2.2. Fibrin architectures of macroporous hydrogels regulated macrophage polarization and deformation

Optimal wound healing depends on the highly regulated transition of macrophages from an M1 pro-inflammatory phenotype to an M2 pro-healing phenotype, which are hallmarks of the progression from injury to repair [6]. Intrigued by the established role of macrophage in biomaterial-induced FBR [24,35–37], we next performed flow cytometry and immunofluorescence staining to evaluate macrophage responses to the materials (Fig. 3A). Muscle and bone tissue collected three days post-implantation, containing MSA-ZW or MSA-DA, were dissociated into single cells and labeled by a series of antibodies as previously reported [38,39]. Flow cytometry analysis revealed that MSA-ZW reduced the number of $CD80^+$ M1 macrophages and increased the $CD206^+$ M2 ratio compared to MSA-DA (Fig. 3B–E), indicating an inhibitory effect on early inflammation. Likewise, the mean grey value of $CD206^+$ fluorescence in MSA-ZW was significantly stronger than in MSA-DA, while iNOS fluorescence intensity showed the opposite pattern (Fig. 3F–I). These findings raise the possibility that the fibrin structure formed by blood-biomaterial contact may regulate macrophage-related inflammation at an early stage, influencing the ultimate outcomes of tissue repair.

To test this hypothesis, macrophages were seeded on MSA-ZW or MSA-DA hydrogels *in vitro*. The hydrogels were first sterilized with 75 % ethanol and irradiated under UV light for over 30 min. Subsequently, the hydrogels were incubated with a physiological concentration of fibrinogen and thrombin at 37 °C for 5 min to mimic fibrin clot formation. RAW264.7 cells were then seeded onto the hydrogels or pretreated with LPS to simulate the early inflammatory environment characteristic of FBR, allowing us to investigate the regulatory role of fibrin networks in macrophage polarization [23] (Fig. 4A). Consistent with *in vivo* findings, RAW264.7 (M0) cells cultured on fibrin-coated MSA-ZW exhibited a higher level of $CD206^+$ M2-type polarization (Fig. 4B), while LPS-induced $CD80^+$ M1 polarization of RAW264.7 cells were mitigated in MSA-ZW contrasting with MSA-DA (Fig. 4C). Additionally, the reduced iNOS fluorescence intensity of M1-type macrophages on MSA-ZW (Fig. 4D) and the significantly downregulated mRNA expression of pro-inflammatory markers such as iNOS, CD80, and IL-6 in MSA-ZW further confirmed its inhibitory effect on macrophage inflammation (Fig. S2). To investigate the underlying mechanisms, we speculated that the morphology of fibrin architectures induced cell deformation, leading to varied inflammatory responses. Scanning electron microscope (SEM) observations revealed that macrophages on MSA-ZW maintained a round shape, while those on MSA-DA exhibited a more elongated shape with more podosomes (Fig. 4E). Phalloidin

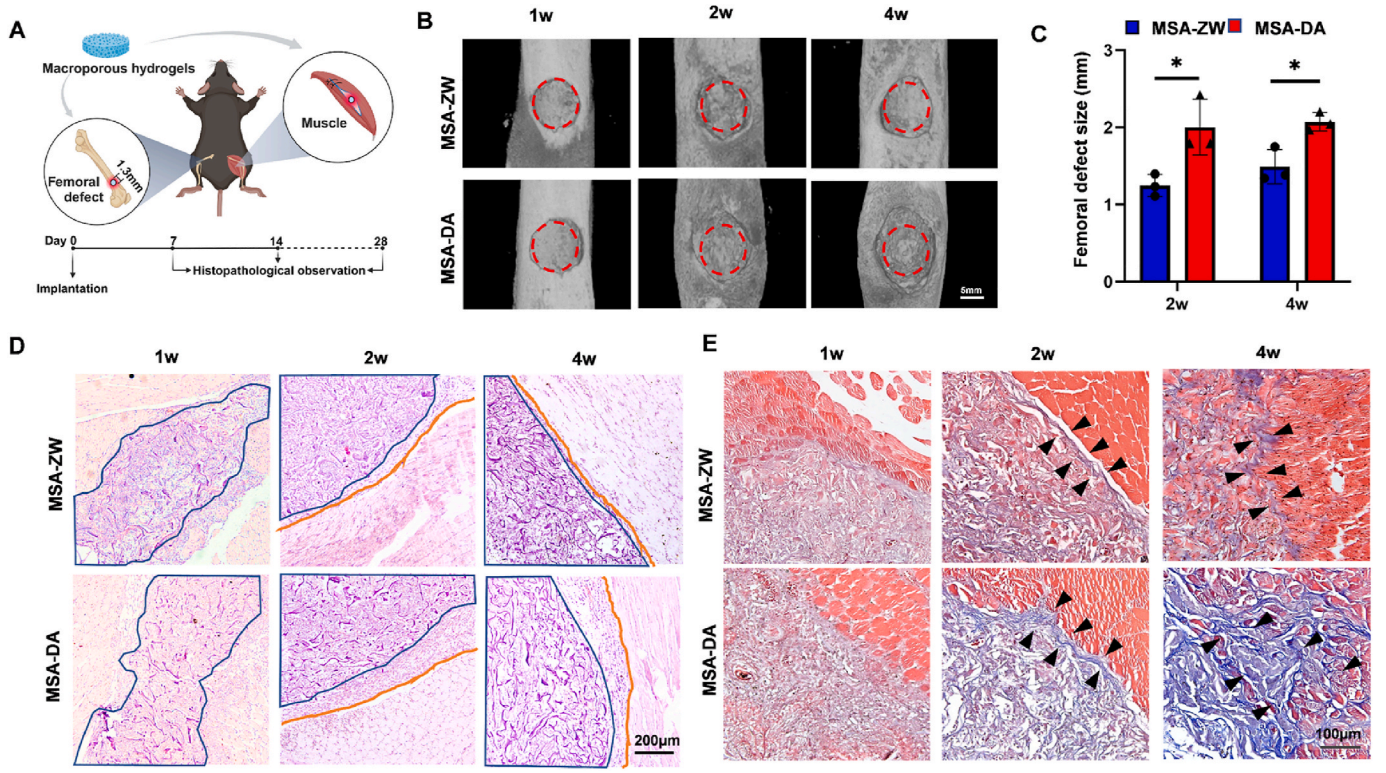

Fig. 2. Foreign body response (FBR) was affected by distinct fibrin network structures in macroporous hydrogels.(A) Schematic diagram of implant surgery of MSA-ZW and MSA-DA implanted in the femoral defect and quadriceps muscle. The experimental timeline for surgery and detection. (B) Representative images of micro-CT images of implantation site of bone at 1, 2, and 4 weeks. The red circle indicated the primary defect range. Scale bar, 5 mm. (C) Quantification of femoral defect size (n = 3, two-tailed Student's t-test, $^*P < 0.05$). (D) Representative images of hematoxylin and eosin (HE) staining of muscle tissue at 1, 2, and 4 weeks post-treatment are presented. The blue outline demarcates the residual material, whereas the orange line delineates the edge of the fibrous capsule. (E) Representative images of Masson's Trichrome staining of muscle at 1, 2, and 4 weeks. The black arrows indicated the collagen fibers.

staining further confirmed the distinct morphologies of macrophages on MSA-ZW and MSA-DA (Fig. 4F). Compared to previous studies that identified fibrin adhesion as inhibiting macrophage inflammatory activation [23], our findings further highlight the structural characteristics of fibrin architectures as key regulators of macrophage activation.

2.3. Adhesion to fibrin architectures triggered mitochondrial mechanosensing in macrophages

Macrophage polarization is commonly associated with morphological changes [40], suggesting that fibrin architectures likely interact with macrophages to elicit signaling pathways linked to the inflammatory response. Integrins, known as biomechanical sensors of the cellular microenvironment, mediate cell adhesion to the ECM and transmit extracellular signals via the phosphorylation of focal adhesion kinase (pFAK) [20]. In macrophages, the integrin types CD18 and CD11b, which form the integrin αMβ2 complex, specifically recognize fibrin [41]. Compared to the MSA-ZW group, gene expression levels of CD11b and CD18 were elevated in the MSA-DA group (Fig. 5A). The protein expression pattern of CD18 mirrored the gene expression levels, and the pFAK/FAK ratio was increased in the MSA-DA group (Fig. 5B). The findings indicate that macrophages cultured in the MSA-DA group, which provides more contact sites, exhibited enhanced activation of the integrin-mediated outside-in signaling pathway compared to those in the MSA-ZW group.

The concept of mitochondrial mechanotransduction, which highlights the role of mitochondria in ECM-cell interactions, has recently been introduced [27]. To further explore the relationship between mitochondria and fibrin architectures, we examined the mitochondrial function of macrophages seeded on microporous hydrogels containing a fibrin network. Mitochondria-generated reactive oxygen species (ROS) and mitochondrial membrane potential (MMP) were detected by mitoSOX production and TMRM staining, respectively. As a result, the ROS and MMP of macrophage mitochondria in MSA-ZW and MSA-DA showed opposite trends, with superior mitochondrial function, lower ROS production, and higher MMP in MSA-ZW (Fig. 5C and D), which was further confirmed by flow cytometry results (Fig. 5E and F). Consistently, the MSA-DA group exhibited decreased ATP content compared to the MSA-ZW group (Fig. 5G). The mRNA expression level of mitochondria-associated genes, including HIF-1α, NDUFB6, SDHA, and VDAC, were significantly different (Fig. S3). These results suggest that mitochondria respond to the morphological changes in macrophages induced by distinct fibrin architectures.

To identify the key regulator of mitochondrial response to the fibrin network, we collected LPS-pretreated macrophages seeded on the MSA-ZW and MSA-DA for 24h for RNA sequencing. Using DeSeq2 for differential expression analysis, we identified 292 differentially expressed genes (DEGs, $p < 0.05$ and $|\text{Fold Change}| \geq 1.5$) (Fig. 5H), and listed the top DEGs of up-regulated and down-regulated (Fig. 5I). Among the DEGs, Tgm2 (encoding Transglutaminase 2) showed a significant fold change and the lowest p-value. The expression differentiation between MSA-ZW and MSA-DA was confirmed at both the gene and protein levels (Figure S4 A and B). The results revealed that Tgm2 was significantly upregulated in the MSA-ZW group compared to the MSA-DA group. Align with our assumptions, GO term enrichment analysis showed that these DEGs were enriched in pathways related to cell adhesion, immune response, and extracellular space (Fig. 5J). Tgm2 is a multifunctional enzyme that exhibits crosslinking, GTPase, cell adhesion, protein disulfide isomerase, kinase, and scaffold activities [42]. Moreover, Tgm2 has been implicated in multiple mitochondrial-associated cell biological

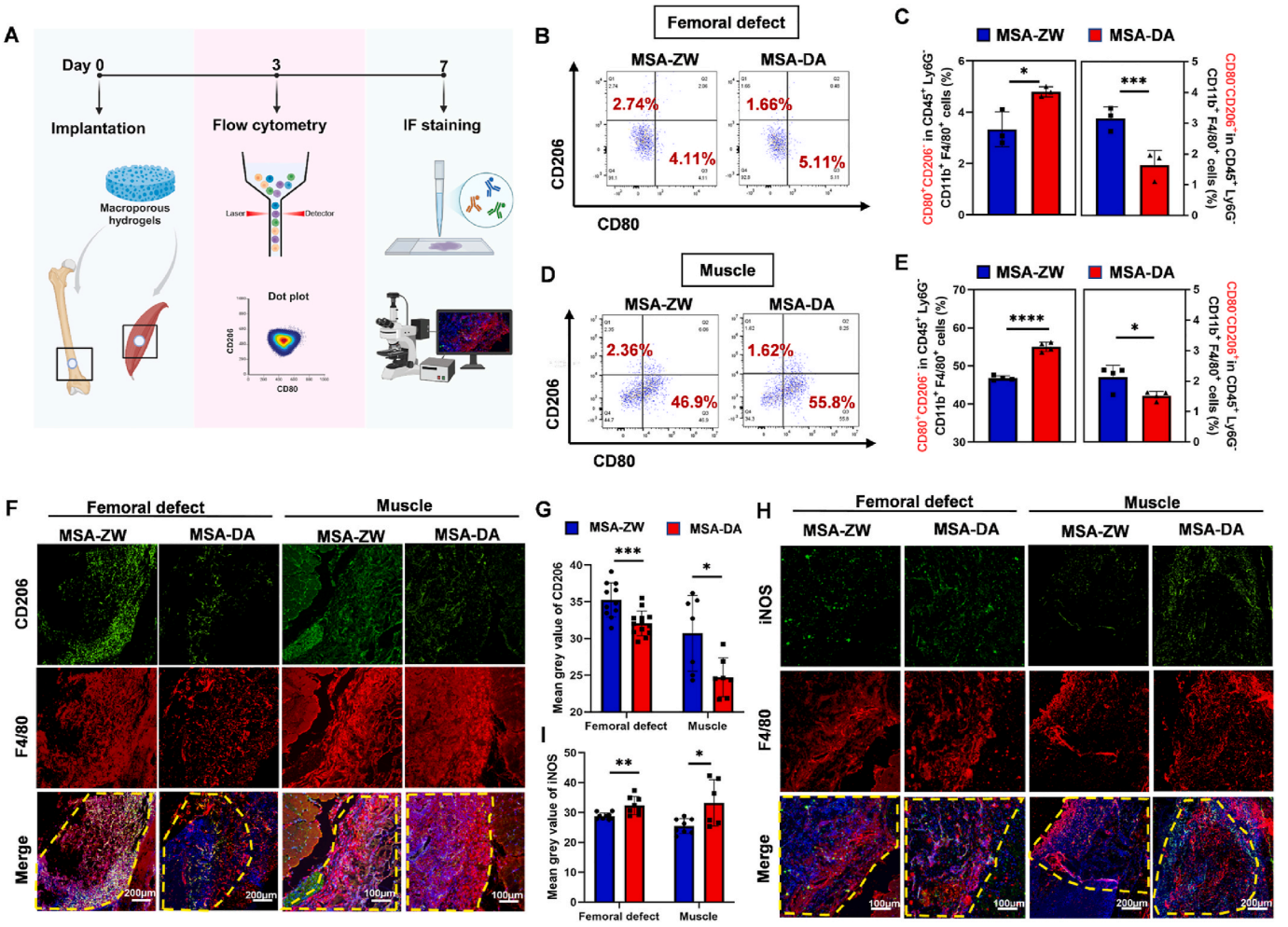

Fig. 3. Macrophages responded differently at the material-tissue interface *in vivo*. (A) Schematic diagram of tissue flow cytometry. The tissues containing MSA-ZW and MSA-DA were digested into single cells. The cell clusters were labeled with fluorescent antibodies and the samples were loading to perform flow cytometry. The results were demonstrated with dot plot. (B–E) Flow cytometry results of tissue flow cytometry. (B) Representative dot plots of $CD80^+$ $CD206^-$ and $CD80^-CD206^+$ cells in femoral defect tissue by flow cytometry. (C) Representative dot plots of $CD80^+$ $CD206^-$ and $CD80^-CD206^+$ cells in muscle tissue by flow cytometry. (D) Quantification of $CD80^+$ $CD206^-$ and $CD80^-CD206^+$ cells in femoral defect tissue (n = 3, two-tailed Student's t-test, $^*P < 0.05$, $^{***}P < 0.001$). (E) Quantification of $CD80^+$ $CD206^-$ and $CD80^-CD206^+$ cells in muscle tissue (n = 3, two-tailed Student's t-test, $^*P < 0.05$, $^{****}P < 0.0001$). (. (F) Representative images of immunostaining of CD206 (green), F4/80 (red), DAPI (blue) in muscle and femoral defect. The yellow frame indicate the residual material. (G) Quantification of CD206 mean grey value. (Femoral defect: n = 10, two-tailed Student's t-test, $^{***}P < 0.001$, muscle: n = 7, two-tailed Student's t-test, $^*P < 0.05$). (H) Representative images of immunostaining of iNOS (green), F4/80 (red), DAPI (blue) in muscle and femoral defect. The yellow frame indicate the residual material (I) Quantification of iNOS mean grey value. (Femoral defect: n = 8, two-tailed Student's t-test, $^{***}P < 0.001$, muscle: n = 6, two-tailed Student's t-test, $^*P < 0.05$).

processes, such as apoptosis, respiration, and mitochondrial dynamics [43–45]. Therefore, Tgm2 may be a crucial gene bridging the fibrin network formed by MSA-ZW and MSA-DA with macrophage mitochondrial mechanosensing.

2.4. *Tgm2 was the pivotal gene in the mitochondrial mechanosensing mechanism*

Both gene and protein expression levels of Tgm2 in LPS-treated macrophages were significantly higher in the MAS-ZW group compared to the MSA-DA group (Figure S4, A and B). Interestingly, inhibition of Tgm2 expression using its inhibitor, Cystamine, did not alter the pFAK/FAK. In contrast, blocking pFAK function with the pFAK inhibitor Defactinib led to a notable increase in the protein level of Tgm2 (Fig. 6A and B). Therefore, this indicated that Tgm2 was positioned downstream of pFAK in macrophages. Based on these results, we hypothesized that the distinct fibrin networks differentiate pFAK activation, which in turn regulated Tgm2 expression in a trans manner (Fig. 6C).

Next, we tried to test whether Tgm2 was a key determinant of the observed differences in the macrophage mitochondrial phenotype. If Tgm2 was responsible for fibrin-mitochondrial communication, the exogenous addition of its inhibitor to macrophages in MSA-ZW should be predicted to a compromised mitochondrial function, thus phenocopying the MSA-DA group. As anticipated, inhibition of Tgm2 obviously elevated ROS production, decreased MMP and reduced ATP content (Fig. 6D–F). These findings confirmed that Tgm2 acts as a protective factor for macrophage mitochondria, alleviating mitochondrial dysfunction.

Since Cystamine is a multifunctional transglutaminase inhibitor, we constructed Tgm2-targeting small interfering RNA (siTgm2) to specifically knock down gene expression, with a universal negative control siRNA (siNC) as a control. Rt-qPCR and Western blot analyses were performed to ensure the efficiency of gene knockdown (Fig. 6G and Fig. S4C). RNA sequencing was then performed to compare the siTgm2 and siNC groups, aiming to explore potential functional pathways. DEGs related to cell adhesion (Itgam), immunity response (Mmp12), fatty acid metabolism (Fads1, Fads2, and Fabp5), and mitochondrial function

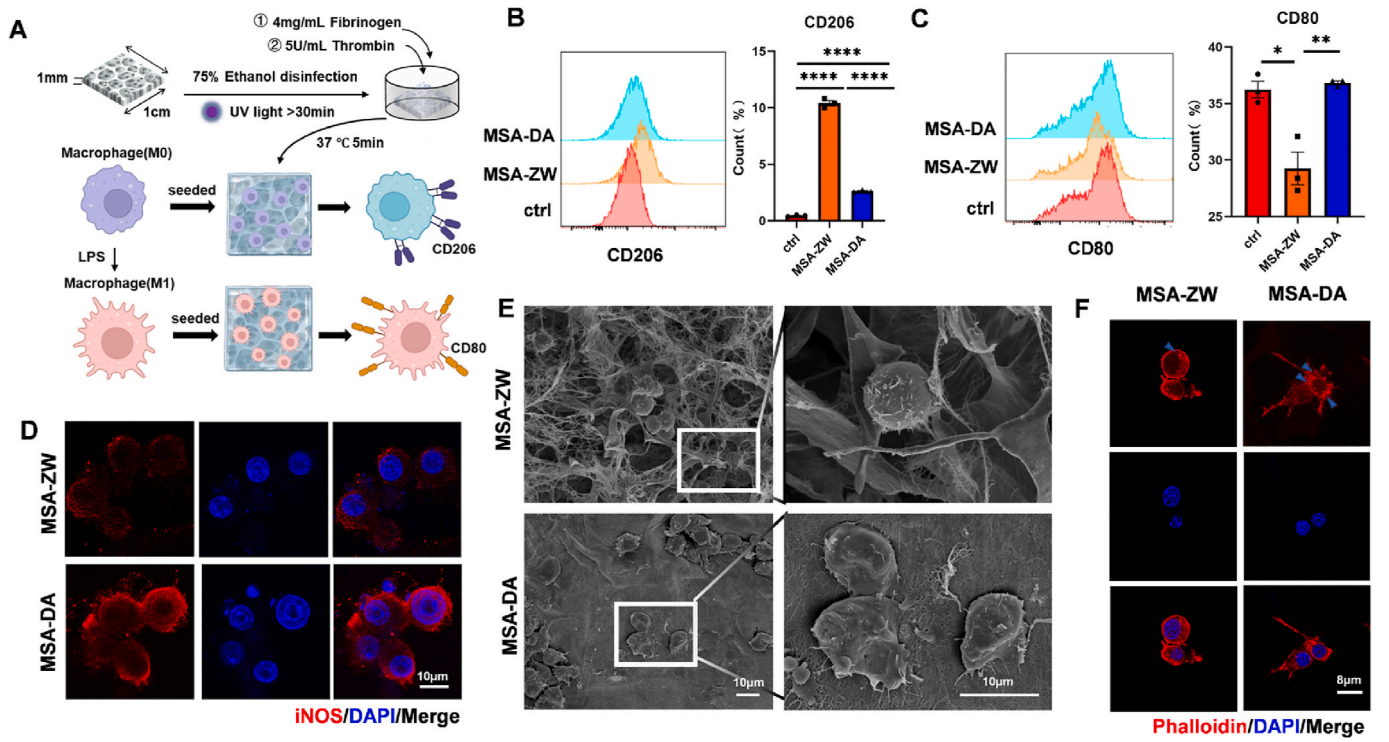

Fig. 4. Macrophages exhibited distinct responses within the fibrin architectures generated by MSA-ZW and MSA-DA *in vitro*.(A) Schematic diagram of RAW264.7 culture strategies: The disinfection of macroporous hydrogels (MSA-ZW and MSA-DA) was achieved using 75 % ethanol and UV light. Subsequently, the macroporous hydrogels were incubated with a solution containing 4 mg/mL Fibrinogen and 5U/mL Thrombin at 37 °C for 5 min. RAW264.7 cells of M0 phenotype were then seeded onto the macroporous hydrogels coated with fibrin networks. The subsequent assessment involved determining the percentage of $CD206^+$ phenotype macrophages (M2) and $CD80^+$ phenotype macrophages (M1). To induce polarization, macrophages (M0) were treated with LPS, transforming them into macrophages (M1). These macrophages (M1) were subsequently seeded onto the macroporous hydrogels with fibrin networks, and the $CD80^+$ phenotype percentage of macrophages (M1) was measured. (G–H) RAW264.7 cells were seeded on MSA-ZW, MSA-DA, and cell culture well plate (ctrl). (B) Representative flow cytometry analysis and quantification of CD206+ phenotype percentage after seeding macrophages (M0) for 24h (n = 3, one-way ANOVA with Tukey's post-test, $^{****}P < 0.0001$). (C) Representative flow cytometry analysis and quantification of $CD80^+$ phenotype percentage (n = 3, one-way ANOVA with Tukey's post-test, $^{*}P < 0.05$, $^{**}P < 0.01$). (D–F) RAW264.7 cells were pretreated with LPS before seeding on the MSA-ZW and MSA-DA. The measurements were taken after culturing for 24 h. (I) Representative images of immunostaining of iNOS (red) and DAPI (blue). (J) Representative images of SEM images. (K) Representative images of immunostaining of phalloidin (red) and DAPI(blue).

(Lcn2, Pdia4, Myc, Rsad2) were identified (Fig. 6H). KEGG pathway enrichment analysis revealed that Tgm2 knock-down significantly altered phenotypes associated with inflammation and fatty acid metabolism (Fig. S5). According to GO pathway enrichment, we further discovered that coenzyme A-related activity was particularly impacted, highlighting the importance of mitochondrial metabolism (Fig. 6I). In summary, the mechanical signaling of fibrin architecture modulated macrophage mitochondrial function through the integrin-pFAK-Tgm2 axis, identifying Tgm2 as a bridge between fibrin architecture and mitochondria.

2.5. *Tgm2 modulated mitochondrial function through PGC1α-mediated mitochondrial biogenesis*

siTgm2 treatment resulted in heightened ROS production both in mitochondrial and in total, along with a higher mitochondrial membrane potential and lower ATP content compared to the siNC group (Fig. 7A–G). The oxygen consumption rate (OCR) was assessed using Seahorse XF cell mito stress test assay (Fig. 7H), and the results revealed significant decreases in basal respiration, ATP production, maximal respiration, and spare respiratory capacity in the siTgm2 group compared to siNC (Fig. 7I). Functioning as a signaling hub within the cell, mitochondria may integrate information from extracellular fibrin architecture and regulate cellular metabolism. Above results indicated that Tgm2 deficiency gave rise to macrophage mitochondrial dysfunction and energy crisis, likely triggering macrophage metabolism reprogramming and eventually a pro-inflammatory phenotype [46].

To investigate how Tgm2 mediated macrophage mitochondrial dysfunction, we directly observed mitochondrial network morphology in the siNC and siTgm2 group (Fig. 7J). The mitochondrial network in the siNC group exhibited a tubular structure surrounding the nucleus and extending throughout the cytoplasm, whereas in the siTgm2 group, the mitochondrial network was reduced in size and significantly aggregated into large clusters. Additionally, increased fragmentation was observed in the siTgm2 cells, with numerous small pieces detached from the main mitochondrial network. Surprisingly, when we evaluate mitochondrial fusion/fission dynamics, only fusion-related genes, mitochondrial fusion protein 2 (Mfn2) and Optic atrophy 1 (Opa1), were downregulated after Tgm2 knockdown, with no changes in their protein levels. Limited changes were also observed in fission-related proteins, including fission protein 1 (Fis1) and dynamin-related protein 1 (Drp1), both in their transcription and translation (Fig. S6). However, a significant reduction in mitochondrial mass was detected in the siTgm2 group, as assessed by relative mtDNA levels (Fig. 7K). Mitochondrial mass is regulated by the dynamic equilibrium between degradation and biogenesis, with Peroxisome proliferator-activated receptor-γ coactivator (PGC)-1α being a major regulator of mitochondrial biogenesis and function [47]. As a proof of concept, we tested the protein expression of PGC1α and mitochondrial transcription factor A (TFAM) and found significantly decreased levels in the siTgm2 group (Fig. 7L and M). Moreover, the level of PGC1α in the MSA-DA group was lower than in MSA-ZW (Fig. S7).

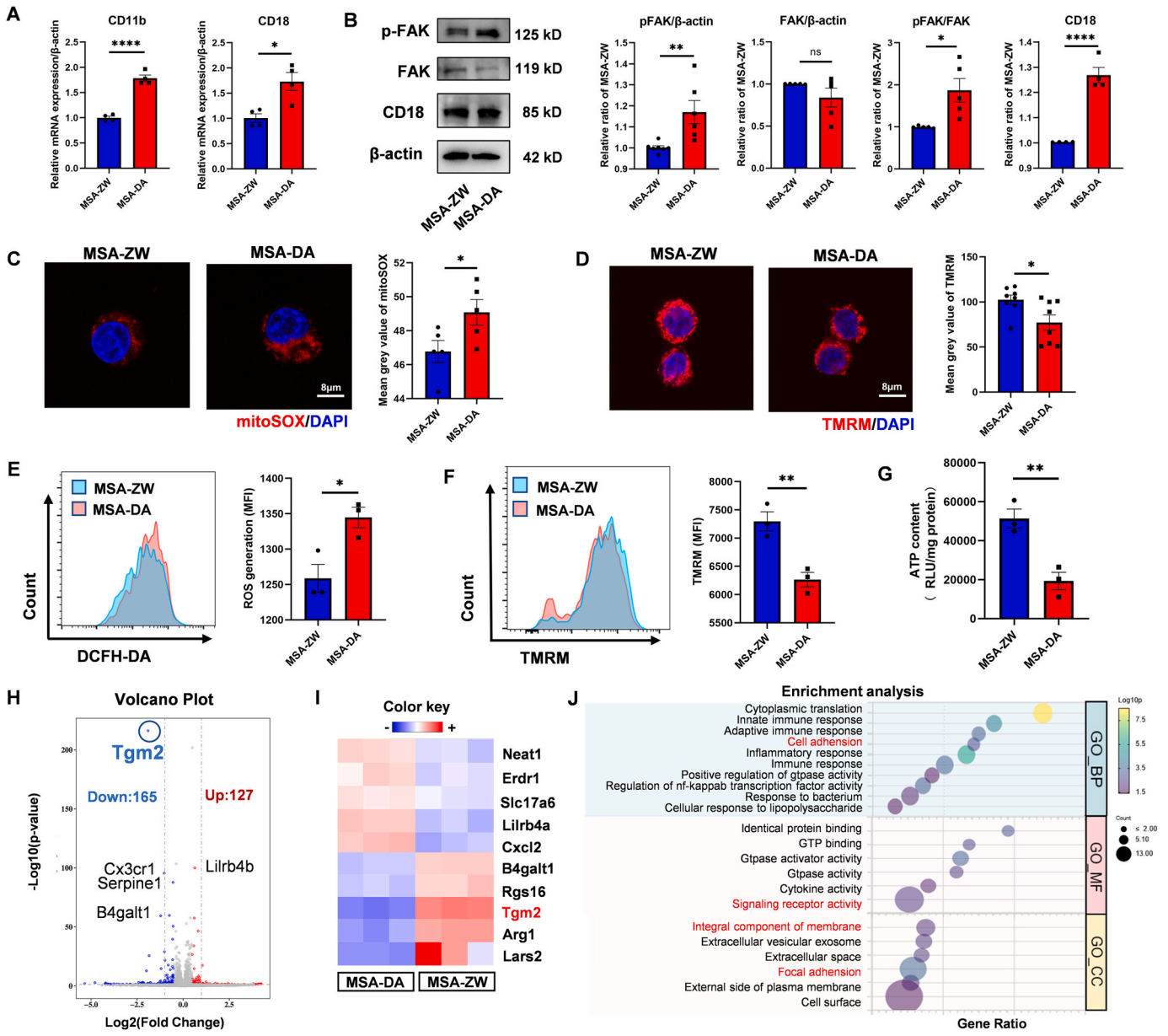

Fig. 5. The adhesive response of macrophages influenced mitochondrial function and TGM2 expression. RAW264.7 cells were pretreated with LPS before seeding on the MSA-ZW and MSA-DA. The measurements were taken after culturing for 24 h. (A) Gene expression analysis of integrin-associated genes CD11b and CD18 (n = 4, two-tailed Student's t-test, $^{*}P < 0.05$, $^{****}P < 0.0001$). (B) Protein expression measured by western blot and quantification of p-FAK, FAK, and CD18 (n = 4–5, two-tailed Student's t-test, $^{*}P < 0.05$, $^{**}P < 0.01$, $^{****}P < 0.0001$, ns, no significant difference). (C) Representative images and quantification of mitoSOX (n = 5, two-tailed Student's t-test, $^{*}P < 0.05$). (D) Representative images and quantification of TMRM (n = 8, two-tailed Student's t-test, $^{*}P < 0.05$). (E) Representative histogram and quantification of DCFH-DA (n = 3, two-tailed Student's t-test, $^{*}P < 0.05$). (F) Representative histogram and quantification of TMRM (n = 3, two-tailed Student's t-test, $^{**}P < 0.01$). (G) ATP content (n = 4, two-tailed Student's t-test, $^{**}P < 0.01$). (H-J) RNA-seq analysis of LPS-pretreated RAM264.7 cells cultured on MSA-ZW and MSA-DA for 24h. (H) The volcano plot illustrates the differentially expressed genes, with Tgm2 identified as one of them. (I) Heat map of gene expression. (J) Biological process (BP), molecular function (MF), and cellular component (CC) pathways of gene ontology (GO) enrichment analysis.

Taken together, the fibrin architecture on the surface of materials, serves as the mechanical microenvironment for macrophages, conveying information about host recognition to foreign bodies. Changes in the morphology of the fibrin network drive macrophage mitochondrial function and behavior, thereby dominating tissue healing outcomes. Our study depicts an uncovered pFAK/Tgm2/PGC1α axis in macrophage mitochondrial mechanotransduction (Scheme 1).

3. Discussion

Tissue repair following biomaterial implantation is a complicated and delicate process that is intricately orchestrated by the immune system. Fibrin networks, formed as a result of the blood clotting process, serve as a primary early trigger for inflammatory responses after implantation [48]. Numerous studies have demonstrated that the outcome of tissue repair is highly dependent on the characteristics of fibrin networks, including their thickness, porosity, permeability, and the number of branching points [49–51]. Interestingly, the spatial cues provided by this provisional extracellular matrix appear to exert unexpected long-term effects over time. Additionally, macrophages play a crucial role in the transition from wound inflammation to tissue repair [52,53]. Given that cell-extracellular matrix mechanotransduction has been shown to modulate cell behaviors [54], macrophage responses to disparate fibrin structures on biomaterial surfaces may determine the

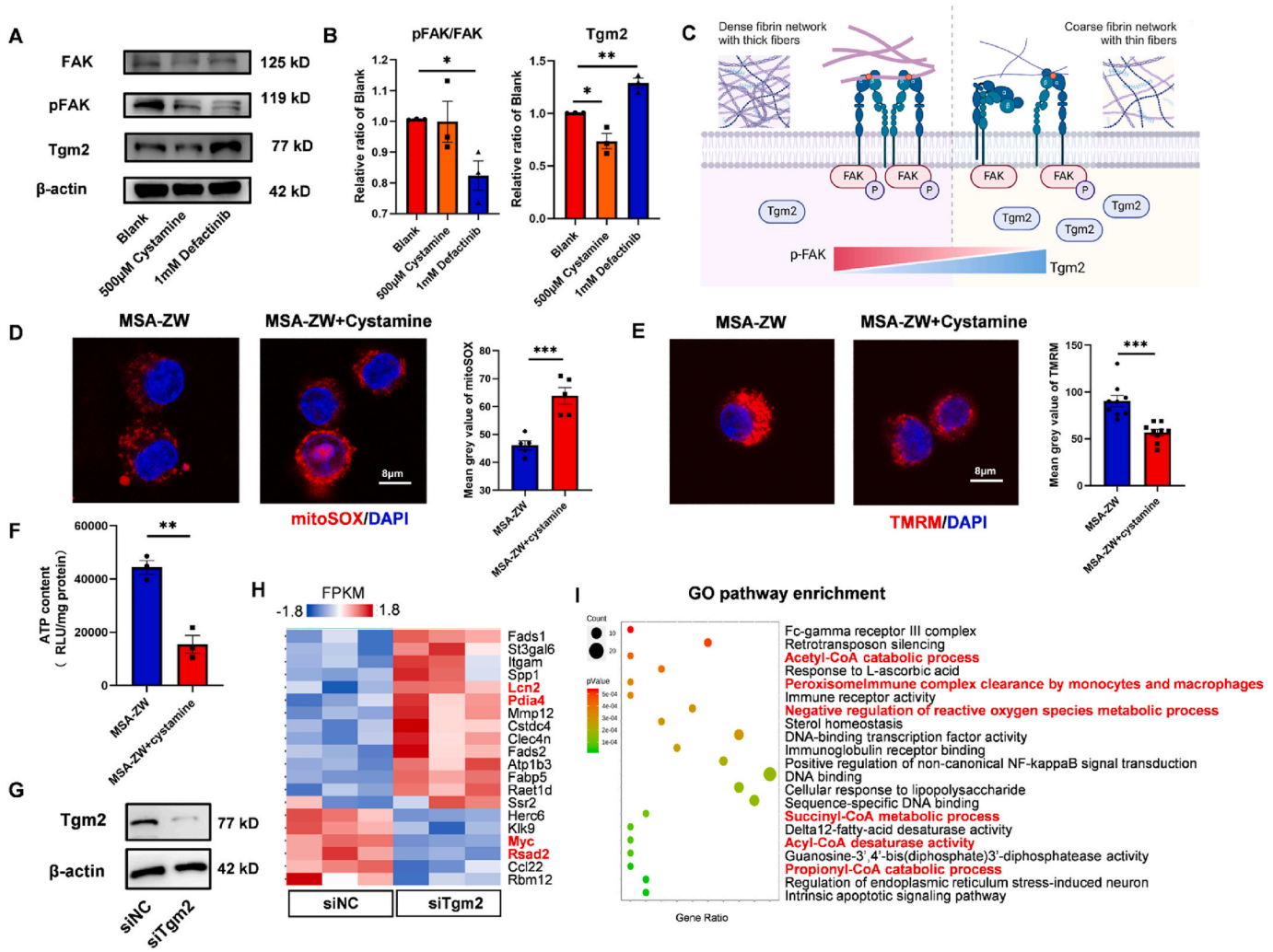

Fig. 6. Tgm2 built connections between fibrin architecture and mitochondria.(A) The protein expression of FAK, pFAK, Tgm2, and β-actin when LPS-pretreated RAW264.7 cells were cultured with blank control (Blank), Tgm2 inhibitor (500 μM Cystamine), and pFAK inhibitor (1 mM Defactinib) for 24h. (B) Quantification of protein expression levels of pFAK/FAK and Tgm2 (n = 3, two-tailed Student's t-test, $*P < 0.05$, $**P < 0.01$). (C) Schematic diagram illustrated the relationship between FAK, pFAK, and Tgm2: Upon formation of a dense fibrin network with thick fibers by MSA-DA, the level of pFAK was upregulated, and the Tgm2 decreased. Conversely, when a coarse fibrin network with thin fibers was formed by MSA-ZW, the pFAK level decreased, while the Tgm2 level was upregulated. (D–F) LPS-pretreated RAM264.7 cells were cultured on MSA-ZW, and MSA-ZW with addition of Cystamine (MSA-ZW + Cystamine) for 24h. (D) Representative images and quantification of mitoSOX (n = 5, two-tailed Student's t-test, $***P < 0.001$). (E) Representative images and quantification of TMRM (n = 8, two-tailed Student's t-test, $***P < 0.001$). (F) ATP content (n = 3, two-tailed Student's t-test, $**P < 0.01$). (G–I) RAW264.7 cells were transfected with non-silencing siRNA as negative control (siNC) and siRNA silencing *Tgm2* (siTgm2). (G) Representative Tgm2 protein expression of siNC and siTgm2. (H) Gene expression heat map of RNA-seq analysis of LPS-pretreated RAM264.7 cells cultured on MSA-ZW for 24h. The items related to mitochondria were highlighted in red. (I) GO pathway enrichment.

host's reaction.

In our study, we developed macroporous hydrogels with differential protein absorption capabilities to generate various fibrin architectures. Our findings revealed that a dense fibrin network, characterized by thick fibers, stimulates an active inflammatory response in macrophages. In contrast, a sparse fibrin network, composed of thin fibers, reduces M1 macrophage polarization and tissue fibrosis. These results align with several studies [35,36], including notable research by W. S. et al. [21], which demonstrated that manipulating the structure of fibrin networks by modifying silica pore size produces thinner, more porous networks that effectively alleviate macrophage inflammation. Our study suggested that modifying the structures of adsorbed host proteins on material surfaces could serve as an effective strategy to mitigate the foreign body response (FBR).

Previous studies have documented that the binding of integrin αMβ2 (i.e., CD11b/CD18 integrin or Mac-1) to fibrin induces phosphorylation of FAK, which is essential for macrophage migration and the subsequent inflammatory response [41,55]. Our study expanded upon current knowledge regarding the interaction between fibrin and macrophages and revealed an unreported role for transglutaminase 2 (Tgm2) in macrophage mechanobiology. Mechanistically, the heterogeneity of fibrin architecture induced differential activation of integrin αMβ2, which, through an inverse relationship, modulated Tgm2 levels. Tgm2, in turn, functions as a regulator of the metabolic characteristics of macrophages, ultimately influencing their polarization and the FBR.

Tgm2 is a highly versatile cellular protein implicated in gene expression, protein homeostasis, cell signaling, autoimmunity, and inflammation [56]. Although Tgm2 is typically considered a profibrotic factor, our results suggest a contrasting role. This discrepancy may arise from differences in its localization and conformation. Extracellular Tgm2 adopts an open, active conformation due to the high Ca^{2+} concentration, facilitating crosslinking and stabilization of the extracellular matrix (ECM), which promotes organ fibrosis [57]. However, intracellular Tgm2 exists in a compact, closed conformation due to GTP binding,

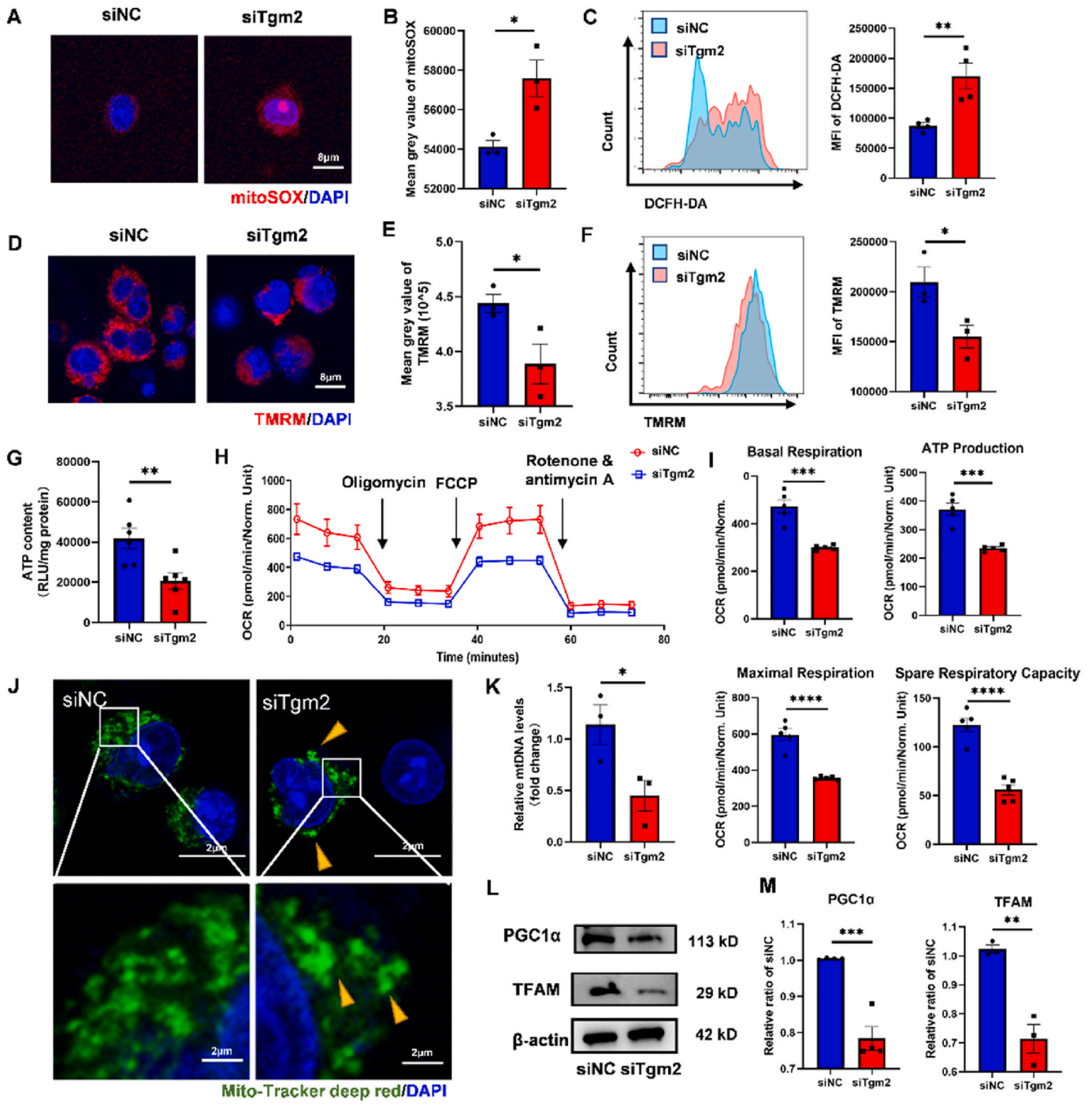

Fig. 7. The knock-down of Tgm2 suppressed PGC1α-mediated mitochondrial biogenesis. RAW264.7 cells were transfected with siNC and siTgm2 and then LPS-pretreated siNC and siTgm2 were seeded on MSA-ZW. (A) Representative images of staining of mitoSOX (red) and DAPI (blue). (B) Quantification of mitoSOX mean grey value (n = 3 individual samples, two-tailed Student's t-test, $^{*}P < 0.05$). (C) Representative flow cytometry analysis and quantification the media fluorescence index (MFI) of DCFH-DA (n = 5, two-tailed Student's t-test, $^{**}P < 0.01$). (D) Representative images of staining of TMRM (red) and DAPI (blue). (E) Quantification of TMRM mean grey value (n = 3 individual sample, two-tailed Student's t-test, $^{*}P < 0.05$). (F) Representative flow cytometry analysis and quantification the MFI of TMRM (n = 3, two-tailed Student's t-test, $^{*}P < 0.05$). (G) ATP content (n = 6, two-tailed Student's t-test, $^{**}P < 0.01$). (H-I) Seahorse XF mito stress test assay. (H) The oxygen consumption rate (OCR) of RAW264.7 (n = 5). (I) Analysis of the basal respiration, ATP production, maximal respiration, and spare respiratory capacity (n = 5, two-tailed Student's t-test, $^{***}P < 0.001$, $^{****}P < 0.0001$). (J) Representative images of staining of Mito-Tracker deep red (green) and DAPI (blue) show the mitochondrial network morphology. The yellow arrows indicate the aggregated mitochondrial clusters. (K) Relative mtDNA levels show the duplication of mtDNA (n = 3, two-tailed Student's t-test, $^{*}P < 0.05$). (M) The protein expression of PGC1α and TFAM. (N) Quantification of protein expression of PGC1α and TFAM (n = 3–4, two-tailed Student's t-test, $^{**}P < 0.001$, $^{***}P < 0.0001$).

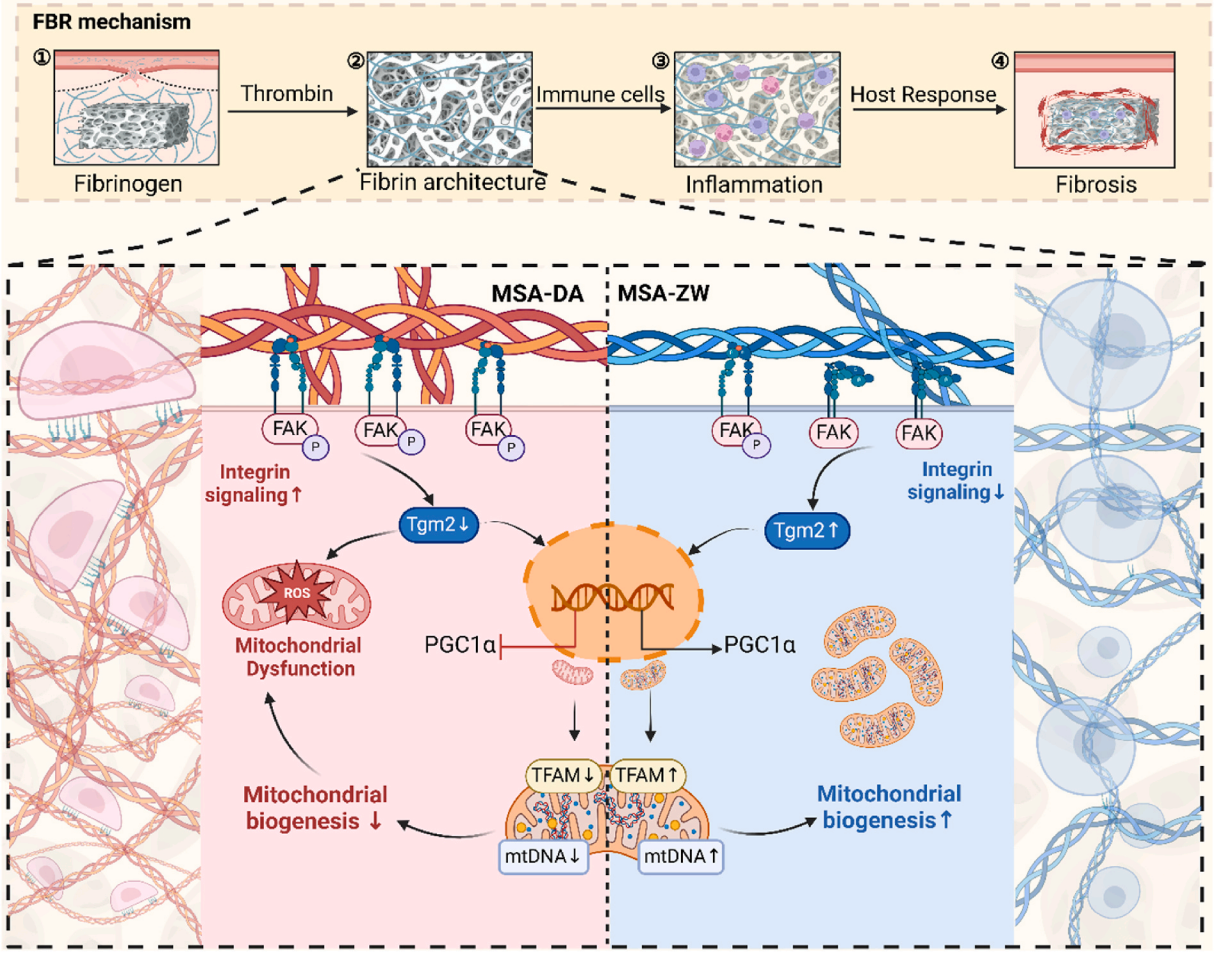

Scheme 1. Constructing heterogeneous fibrin architectures deciphers macrophage mitochondrial mechanosensing to thwart the FBR. Fibrin architectures formed on macroporous hydrogels define the mechanical microenvironments of macrophages and modulate FBR. Differential activation of integrins, induced by the conformational variations in fibrin networks, regulates macrophage mitochondrial mechanosensing in a Tgm2-dependent manner.

lacking transamidation activity and exhibiting abundant protein interactions [56,58]. It has been reported that Tgm2 is more abundant in round macrophages compared to spindle-shaped ones, and its inhibition triggers a pro-inflammatory phenotype [59]. Furthermore, Tgm2 plays a role in stabilizing protein complexes involved in mitochondrial homeostasis and interacts with mitochondrial dynamic proteins, thereby protecting cells from stress [60–62]. Herein, we endowed Tgm2 with a novel role in PGC1α-mediated macrophages mitochondrial biogenesis, a process critical for maintaining mitochondrial function and regulating the energy demands of the cell. While our findings provide valuable insights, the precise molecular mechanisms by which Tgm2 regulates mitochondrial biogenesis remain to be fully elucidated, representing an exciting avenue for future research.

The mechanosensitive properties of mitochondria have emerged as an area of considerable interest. The cell-ECM signaling pathway is transmitted through cytoskeletal deformation, which is essential for mitochondrial distribution, morphology, dynamics, energy metabolism, and the expression of mitochondrial-related genes [63–67]. It is intriguing to speculate that, during the evolution of eukaryotes, mitochondrial endosymbiosis may have reversed fundamental sensory processes, such as the ability to sense morphological changes. These developmental remnants were inherited by modern cells, where they influence cell morphology as a signal for mitochondrial function. Our findings supported that mechanical microenvironments can affect mitochondrial function by regulating gene transcription process. RNA-seq analysis indicates a potential link to mitochondrial lipid metabolism, warranting further investigation.

In summary, our study demonstrates that the mechanical cues provided by fibrin architecture are sufficient to modulate macrophage mitochondrial functions, a process regulated by integrin signaling and downstream Tgm2 levels. We introduce a novel perspective on the FBR, highlighting the importance of fibrin network structure in biomaterial implant design. We also anticipate future applications that explore the impact of Tgm2 and mitochondrial mechanotransduction on the FBR. However, it is important to note that our study focused primarily on pure fibrin scaffolds. Fibrin clot formation *in vivo* is a highly coordinated and complex process, and the structure of fibrin networks can be influenced by several enzymes and modulators, such as thrombin and plasminogen [68]. In addition to serving as a provisional matrix for cells, fibrin clots capture various growth factors and cytokines, which significantly influence the outcome of wound healing [69]. Thus, further investigation is needed to fully understand this unique matrix and achieve optimal biocompatibility.

4. Experimental methods

4.1. Synthesis of hydrogels

Detailed synthesis procedure was provided in the supplementary materials.

4.1.1. MSA-ZW

ZW-SA (0.4 g) was dissolved in 50 mL of a buffer solution containing 100 mM MES. N-hydroxysuccinimide (0.35 g, 1 eq) and 1-ethyl-(3-dimethylaminopropyl) carbodiimide (1.3 eq) were added, and the mixture was stirred for 10 min to activate the carboxylic acid groups of sodium alginate. Subsequently, 2-aminoethyl methacrylate hydrochloride (0.66 g, 1.1 eq) was added, and the solution was stirred at room temperature for 24 h. The resulting solution was dialyzed using 8000–14000 Da dialysis bags for three days and then freeze-dried to yield MSA-ZW. NMR analysis confirmed a modification degree of approximately 47.94 %.

4.1.2. MSA

Sodium alginate (0.5 g) was dissolved in 60 mL of a buffer solution containing 100 mM 2-morpholineethanesulfonic acid (MES). After complete dissolution, N-hydroxysuccinimide (0.4375 g, 1 eq) and 1-ethyl-(3-dimethylaminopropyl) carbodiimide (0.95 g, 1.3 eq) were added and stirred for 10 min. 2-Aminoethyl methacrylate hydrochloride (0.825 g, 1.1 eq) was then added, and the reaction was stirred at room temperature for 24 h. The resulting solution was dialyzed using 8000–14000 Da molecular weight cutoff dialysis bags for three days and freeze-dried. NMR analysis indicated that the degree of modification of the starting alginate was approximately 49.29 %.

4.1.3. MSA-DA

MSA (0.4 g) was dissolved in 50 mL of a buffer solution containing 100 mM MES. N-hydroxysuccinimide (0.145 g, 1 eq) and 1-ethyl-(3-dimethylaminopropyl) carbodiimide (0.2425 g, 1 eq) were added, and the mixture was purged with nitrogen gas for 30 min at room temperature. Dopamine hydrochloride (0.58 g, 3 eq) was then added, and the reaction was stirred overnight at room temperature. NMR analysis confirmed a modification degree of approximately 21.56 %.

4.2. Characterization of hydrogels

4.2.1. Morphology

The morphology of the hydrogels (with or without fibrin) was observed using a scanning electron microscopy (SEM; VEGA3, Czech Republic) at an operating voltage of 7 kV. The porosity and branch thickness of the fibrin network were analyzed using ImageJ (National Institutes of Health, USA).

4.2.2. 1H nuclear magnetic resonance

MSA-ZW and MSA-DA were detected using a nuclear magnetic resonance (NMR) instrument (ADVANCE NEO 400, USA) after dissolution in deuterated heavy water. The modification rate was obtained by calculating the hydrogen peak area of the modified MSA-ZW and MSA-DA.

4.2.3. Elastic modulus

The mechanical properties of the hydrogels were measured using a universal testing machine (Instron 5966, USA). For the compression test, the hydrogel samples were prepared as cylinders with a diameter of 1 mm and a height of 5 mm, and the compression speed was set to 2 mm/min. The modulus of the hydrogel was calculated from the initial linear slope of the stress-strain curve.

4.2.4. Swelling ratio

MSA-ZW and MSA-DA were prepared with a volume of 0.5 mL, lyophilized, and their initial weights were recorded (W0). All samples were then immersed in PBS at 37 °C, and their weights at different time points after immersion were recorded (Wt). The swelling ratios of the hydrogels were calculated using the following formula:

$$\text{Swelling ratio} = \frac{Wt - W0}{W0} \times 100\%$$

4.3. Construction of fibrin networks and cell culture

Both 75 μL of fibrinogen (4 mg/mL, attenuated with PBS) and thrombin (5u/mL, attenuated with PBS) were added to MSA-ZW/MSA-DA and incubated in 37 °C for 5 min. The RAW264.7 cells were cultured in high-glucose DMEM containing of 10 % FBS (Gibco, USA) and 1 % penicillin and streptomycin. RAW264.7 cells were seeded with a density of 2×10^5 cells/mL. SEM was used to observe the surface features of MSA-ZW/MSA-DA with or without fibrin networks and cellular morphology of seeded macrophages.

4.4. Animal models

All animal experiments in this study were approved by the Ethics Committee of Zhejiang University (No. ZJU20240905) and conducted following laboratory animal care and usage guidelines. C57BL/6 mice (9 weeks, female) used in the study were provided by the Experimental Animal Center of Zhejiang University. The mice were subsequently assigned to one of two treatment groups: in the MSA-ZW group, the wound site was treated with MSA-ZW hydrogel; in the MSA-DA group, the wound site was treated with MSA-DA hydrogel. After sterilization, two models were constructed: Quadriceps femoris muscle FBR model and Distal femoral defect model. Detailed animal model procedures were described in the Supporting Information. All mice were fed and maintained in a room with a light/dark cycle of 12 h and a stable temperature and humidity (25 °C). The mice were euthanized at 3 days, 1 week, 2 weeks, and 4 weeks post-implantation for flow cytometry analysis or histopathological examination.

4.5. In vivo and in vitro flow cytometry

Following enzymatic dissociation of tissues, the suspension was filtered by a 40 μm mesh to separate single cells. Zombie-BV510 (BioLegend, 1:1000) was first applied to exclude dead cells. After one-time washing, cells were resuspended in a staining buffer and further stained with CD45-PERCY7 (Dakewe Biotech, 1:200), Ly6G-PE (Dakewe Biotech, 1:200), CD11b-FITC (Dakewe Biotech, 1:200), F4/80-BV785 (Dakewe Biotech, 1:200) and CD80-PECY5 (Dakewe Biotech, 1:200) for 20 min at room temperature. For *in vitro* flow cytometry, harvested RAW264.7 cells were incubated with CD80-PECY5 (1:200) at room temperature for 30 min. For intracellular staining of CD206, cells were fixed and permeabilized, and incubated with CD206-APC on ice for 30 min. After additional washings, cells were analyzed by flow cytometry immediately.

4.6. Micro-CT analysis

Femur defects were divided into MSA-DA and MSA-ZW groups and the defect sizes were determined by micro-CT (Bruker, Skyscan 1276) with the following conditions: tube voltage of 45 kV, tube current of 200 mA.

4.7. Western blotting

Cells blown down by PBS from the hydrogels were filtered by a sieve. Total intracellular proteins were extracted using a pre-cooled RIPA lysis buffer containing PMSF (Beyotime, 1:100) and qualified via BCA assay (Beyotime). The protein was isolated with 10 % SDS-PAGE at a constant pressure of 100V for 60 min. The isolated proteins were transferred to the PVDF membrane (Millipore) at a constant current of 350 mA for 70 min, and the PVDF membrane was activated by rinsing with methanol for 1 min in advance. The membrane was blocked with TBST containing 5 % skim milk at room temperature for 1 h, followed by overnight incubation at 4 °C using commonly utilized antibodies: anti-pFAK (Cell Signaling Technology, 1:1000), anti-FAK (Affinity, 1:1000), anti-CD18 (Abclonal, 1:1000), anti-TGM2 (Abclonal, 1:1000), and anti-β-actin

(Abclonal, 1:5000). Subsequent iterations comprised multiple PVDF membrane rinsing steps, post which they were further incubated with the appropriate horseradish peroxidase-conjugated secondary antibodies (Abclonal, 1:5000) for 1 h at room temperature. Signals were detected using enhanced chemiluminescence reagents (Applygen) and quantified by Fuji software.

4.8. Metabolic analysis by seahorse

Metabolic analysis was performed utilizing the XFe96 extracellular flux analyzer (Seahorse Bioscience). Processed RAW264.7 (2×10^4 cells per well) were inoculated onto an XFe96 Seahorse microplate pre-filled with a complete culture medium. Subsequently, the medium in each well was replaced with XF assay buffer supplemented with 10 mM glucose, 1 mM sodium pyruvate, and 2 mM L-glutamine. The plate was then equilibrated at 37 °C in a carbon dioxide-free incubator for 1 h. The assay was conducted through the sequential injection of oligomycin (1.5 μM), FCCP (1.0 μM), and rotenone/antimycin A (0.5 μM). Data were normalized to the total protein concentration in each well. Analysis of the data was performed using Seahorse Wave software version 2.6.1.

4.9. Plasmid transfection

Transfection to silence TGM2 expression was achieved using siRNA and Lipofectamine 3000 (Invitrogen). Three distinct siRNA constructs (Sangon) were evaluated, and the most potent one was selected for subsequent experiments. Briefly, RAW264.7 cells were seeded in a 6-well plate, and after 24 h, transfection complexes and siRNA were added. The content of siTGM2 and siNC was 75 pmol per well. Cells were lysed for qPCR after 24h and for western blot analysis after 48 h.

4.10. RNA-sequencing

The data on cranial defects were sourced from the Genome Sequence Archive (GSA)database under the accession number GSE286900. Raw sequences were transformed into clean reads after data processing. These clean reads were then mapped to the reference genome sequence. Hisat2 tools soft were used to map with the reference genome. Gene function was annotated based on the following databases: Pfam (Protein family); KO (KEGG Ortholog database); GO (Gene Ontology). Differential expression analysis of two conditions/groups was performed using the DESeq2 R package (1.26.0). DESeq2 provide statistical routines for determining differential expression in digital gene expression data using a model based on the negative binomial distribution. The resulting *P* values were adjusted using the Benjamini and Hochberg's approach for controlling the false discovery rate. Genes with DEG, $p < 0.05$ & | Fold Change |≥1.5, found by DESeq2 were assigned as differentially expressed.

4.11. Statistical analysis

GraphPad Prism 9.0 software and Excel for data analysis. Data is expressed as mean ± SD. Statistical significance was determined by two-tailed Student's t-test or one-way analysis of variance (ANOVA) with multiple comparison tests of more groups. $p < 0.05$ was considered statistically significant, $^{*}P < 0.05$; $^{**}P < 0.01$; $^{***}P < 0.001$; $^{****}P < 0.0001$; ns, not significant.

CRediT authorship contribution statement

Bicong Gao: Writing – review & editing, Writing – original draft, Visualization, Methodology, Investigation, Data curation, Conceptualization. **Haifeng Ni:** Writing – review & editing, Writing – original draft, Methodology. **Junhong Lai:** Writing – review & editing, Writing – original draft, Visualization. **Ning Gao:** Writing – review & editing, Writing – original draft, Methodology, Funding acquisition. **Xinxin Luo:** Writing – review & editing, Writing – original draft, Methodology. **Ying Wang:** Writing – review & editing, Writing – original draft, Funding acquisition. **Yani Chen:** Writing – review & editing, Writing – original draft, Visualization, Methodology. **Jiaying Zhao:** Writing – review & editing, Writing – original draft, Data curation. **Zhou Yu:** Writing – review & editing, Writing – original draft, Methodology. **Jing Zhang:** Writing – review & editing, Writing – original draft, Funding acquisition, Conceptualization. **Wenjin Cai:** Writing – review & editing, Writing – original draft, Methodology, Funding acquisition, Formal analysis, Data curation, Conceptualization. **Guoli Yang:** Writing – review & editing, Writing – original draft, Supervision, Funding acquisition, Conceptualization.

Ethics approval and consent to participate

All animal experiments in this study were approved by the Ethics Committee of Zhejiang University (No. ZJU20240905) and conducted laboratory animal care and usage guidelines.

Declaration of competing interest

The authors declare that they have no known competing financial interests or personal relationships that could have appeared to influence the work reported in this paper.

Acknowledgements

B.G., H.N., and J.L. contributed equally to this work. This work was supported by the National Natural Science Foundation of China (82271001 to G.Y.), the National Natural Science Foundation of China (82370928 to Y.W.), the National Natural Science Foundation of China (82301018 to W.C.), the National Natural Science Foundation of China (82401158 to N.G.), and the National Natural Science Foundation of China (52073256 to J.Z.).

Appendix A. Supplementary data

Supplementary data to this article can be found online at https://doi.org/10.1016/j.bioactmat.2025.04.022.

References

[1] X. Feng, J. Gu, Y. Zhou, Primary total hip arthroplasty failure: aseptic loosening remains the most common cause of revision, Am J Transl Res 14 (2022) 7080–7089.
[2] S.A. Sabah, R. Knight, A. Alvand, D.W. Murray, S. Petrou, D.J. Beard, A.J. Price, No exponential rise in revision knee replacement surgery over the past 15 years: an analysis from the National Joint Registry, Osteoarthr. Cartil. 30 (2022) 1670–1679, https://doi.org/10.1016/j.joca.2022.08.016.
[3] C.J. Coroneos, J.C. Selber, A.C.I. Offodile, C.E. Butler, M.W. Clemens, US FDA breast implant postapproval studies: long-term outcomes in 99,993 patients, Ann. Surg. 269 (2019) 30, https://doi.org/10.1097/SLA.0000000000002990.
[4] H. Headon, A. Kasem, K. Mokbel, Capsular contracture after breast augmentation: an update for clinical practice, Archiv. Plastic Surg. 42 (2022) 532–543, https://doi.org/10.5999/aps.2015.42.5.532.
[5] J. Keiler, M. Schulze, M. Sombetzki, T. Heller, T. Tischer, N. Grabow, A. Wree, D. Bänsch, Neointimal fibrotic lead encapsulation – Clinical challenges and demands for implantable cardiac electronic devices, J. Cardiol. 70 (2017) 7–17, https://doi.org/10.1016/j.jjcc.2017.01.011.
[6] K.E. Martin, A.J. García, Macrophage phenotypes in tissue repair and the foreign body response: implications for biomaterial-based regenerative medicine strategies, Acta Biomater. 133 (2021) 4–16, https://doi.org/10.1016/j.actbio.2021.03.038.
[7] Y. Chen, Z. Luo, W. Meng, K. Liu, Q. Chen, Y. Cai, Z. Ding, C. Huang, Z. Zhou, M. Jiang, L. Zhou, Decoding the "fingerprint" of implant materials: insights into the foreign body reaction, Small 20 (2024) 2310325, https://doi.org/10.1002/smll.202310325.
[8] T. ten Brink, F. Damanik, J.I. Rotmans, L. Moroni, Unraveling and harnessing the immune response at the cell–biomaterial interface for tissue engineering purposes, Adv. Healthcare Mater. 13 (2024) 2301939, https://doi.org/10.1002/adhm.202301939.

[9] Z. L, C. Z, B. T, C. L, E.-M. Jr, I. C, R. Bd, J. S, Zwitterionic hydrogels implanted in mice resist the foreign-body reaction, Nat. Biotechnol. 31 (2013), https://doi.org/10.1038/nbt.2580.
[10] Q. Liu, A. Chiu, L.-H. Wang, D. An, M. Zhong, A.M. Smink, B.J. de Haan, P. de Vos, K. Keane, A. Vegge, E.Y. Chen, W. Song, W.F. Liu, J. Flanders, C. Rescan, L. G. Grunnet, X. Wang, M. Ma, Zwitterionically modified alginates mitigate cellular overgrowth for cell encapsulation, Nat. Commun. 10 (2019) 5262, https://doi.org/10.1038/s41467-019-13238-7.
[11] D. Zhang, Q. Chen, Y. Bi, H. Zhang, M. Chen, J. Wan, C. Shi, W. Zhang, J. Zhang, Z. Qiao, J. Li, S. Chen, R. Liu, Bio-inspired poly-DL-serine materials resist the foreign-body response, Nat. Commun. 12 (2021) 5327, https://doi.org/10.1038/s41467-021-25581-9.
[12] X. Zhou, W. Cao, Y. Chen, Z. Zhu, Y. Chen, Y. Ni, Z. Liu, F. Jia, Z. Lu, Y. Ye, H. Han, K. Yao, W. Liu, X. Wei, S. Chen, Y. Wang, J. Ji, P. Zhang, Poly(Glutamic Acid-Lysine) hydrogels with alternating sequence resist the foreign body response in rodents and non-human primates, Adv. Sci. 11 (2024) 2308077, https://doi.org/10.1002/advs.202308077.
[13] X. Xie, J.C. Doloff, V. Yesilyurt, A. Sadraei, J.J. McGarrigle, M. Omami, O. Veiseh, S. Farah, D. Isa, S. Ghani, I. Joshi, A. Vegas, J. Li, W. Wang, A. Bader, H.H. Tam, J. Tao, H. Chen, B. Yang, K.A. Williamson, J. Oberholzer, R. Langer, D.G. Anderson, Reduction of measurement noise in a continuous glucose monitor by coating the sensor with a zwitterionic polymer, Nat. Biomed. Eng. 2 (2018) 894–906, https://doi.org/10.1038/s41551-018-0273-3.
[14] W.-H. Chen, T.-Y. Liao, H. Thissen, W.-B. Tsai, One-step aminomalononitrile-based coatings containing Zwitterionic copolymers for the reduction of biofouling and the foreign body response, ACS Biomater. Sci. Eng. 5 (2019) 6454–6462, https://doi.org/10.1021/acsbiomaterials.9b00871.
[15] R. Chang, J.-L. Chen, G.-Y. Zhang, Y. Li, H.-Z. Duan, S.-Z. Luo, Y.-X. Chen, Intrinsically disordered protein condensate-modified surface for mitigation of biofouling and foreign body response, J. Am. Chem. Soc. 144 (2022) 12147–12157, https://doi.org/10.1021/jacs.2c02677.
[16] L. Vroman, A.L. Adams, G.C. Fischer, P.C. Munoz, Interaction of high molecular weight kininogen, factor XII, and fibrinogen in plasma at interfaces, Blood 55 (1980) 156–159.
[17] A.S. Wolberg, Fibrinogen and fibrin: synthesis, structure, and function in health and disease, J. Thromb. Haemostasis 21 (2023) 3005–3015, https://doi.org/10.1016/j.jtha.2023.08.014.
[18] J.Y. Hsieh, T.D. Smith, V.S. Meli, T.N. Tran, E.L. Botvinick, W.F. Liu, Differential regulation of macrophage inflammatory activation by fibrin and fibrinogen, Acta Biomater. 47 (2017) 14–24, https://doi.org/10.1016/j.actbio.2016.09.024.
[19] A. Balabiyev, N.P. Podolnikova, J.A. Kilbourne, D.P. Baluch, D. Lowry, A. Zare, R. Ros, M.J. Flick, T.P. Ugarova, Fibrin polymer on the surface of biomaterial implants drives the foreign body reaction, Biomaterials 277 (2021) 121087, https://doi.org/10.1016/j.biomaterials.2021.121087.
[20] J.Z. Kechagia, J. Ivaska, P. Roca-Cusachs, Integrins as biomechanical sensors of the microenvironment, Nat. Rev. Mol. Cell Biol. 20 (2019) 457–473, https://doi.org/10.1038/s41580-019-0134-2.
[21] W. S, S. Z, X. L, S. M, Z. P, H. P, Z. L, S. X, L. Z, Z. G, C. Z, Mesopore controls the responses of blood clot-immune complex via modulating fibrin network, Adv. Sci. 9 (2022), https://doi.org/10.1002/advs.202103608.
[22] N. Jain, J. Moeller, V. Vogel, Mechanobiology of macrophages: how physical factors coregulate macrophage plasticity and phagocytosis, Annu. Rev. Biomed. Eng. 21 (2019) 267–297, https://doi.org/10.1146/annurev-bioeng-062117-121224.
[23] V.S. Meli, H. Atcha, P.K. Veerasubramanian, R.R. Nagalla, T.U. Luu, E.Y. Chen, C. F. Guerrero-Juarez, K. Yamaga, W. Pandori, J.Y. Hsieh, T.L. Downing, D. A. Fruman, M.B. Lodoen, M.V. Plikus, W. Wang, W.F. Liu, YAP-mediated mechanotransduction tunes the macrophage inflammatory response, Sci. Adv. 6 (2020), https://doi.org/10.1126/sciadv.abb8471 eabb8471.
[24] Y. Ni, H. Qi, F. Zhang, S. Jiang, Q. Tang, W. Cai, W. Mo, R.J. Miron, Y. Zhang, Macrophages modulate stiffness-related foreign body responses through plasma membrane deformation, Proc. Natl. Acad. Sci. U. S. A. 120 (2023) e2213837120, https://doi.org/10.1073/pnas.2213837120.
[25] H. Atcha, A. Jairaman, J.R. Holt, V.S. Meli, R.R. Nagalla, P.K. Veerasubramanian, K.T. Brumm, H.E. Lim, S. Othy, M.D. Cahalan, M.M. Pathak, W.F. Liu, Mechanically activated ion channel Piezo1 modulates macrophage polarization and stiffness sensing, Nat. Commun. 12 (2021) 3256, https://doi.org/10.1038/s41467-021-23482-5.
[26] R.G. Scheraga, S. Abraham, K.A. Niese, B.D. Southern, L.M. Grove, R.D. Hite, C. McDonald, T.A. Hamilton, M.A. Olman, TRPV4 mechanosensitive ion channel regulates lipopolysaccharide-stimulated macrophage phagocytosis, J. Immunol. 196 (2016) 428–436, https://doi.org/10.4049/jimmunol.1501688.
[27] P. Romani, G. Benedetti, M. Cusan, M. Arboit, C. Cirillo, X. Wu, G. Rouni, V. Kostourou, M. Aragona, C. Giampietro, P. Grumati, G. Martello, S. Dupont, Mitochondrial mechanotransduction through MIEF1 coordinates the nuclear response to forces, Nat. Cell Biol. 26 (2024) 2046–2060, https://doi.org/10.1038/s41556-024-01527-3.
[28] K.M. Tharp, R. Higuchi-Sanabria, G.A. Timblin, B. Ford, C. Garzon-Coral, C. Schneider, J.M. Muncie, C. Stashko, J.R. Daniele, A.S. Moore, P.A. Frankino, S. Homentcovschi, S.S. Manoli, H. Shao, A.L. Richards, K.-H. Chen, J. ten Hoeve, G. M. Ku, M. Hellerstein, D.K. Nomura, K. Saijo, J. Gestwicki, A.R. Dunn, N.J. Krogan, D.L. Swaney, A. Dillin, V.M. Weaver, Adhesion-mediated mechanosignaling forces mitohormesis, Cell Metab. 33 (2021) 1322–1341.e13, https://doi.org/10.1016/j.cmet.2021.04.017.
[29] C. Miceli, F. Roccio, L. Penalva-Mousset, M. Burtin, C. Leroy, I. Nemazanyy, N. Kuperwasser, M. Pontoglio, G. Friedlander, E. Morel, F. Terzi, P. Codogno, N. Dupont, The primary cilium and lipophagy translate mechanical forces to direct metabolic adaptation of kidney epithelial cells, Nat. Cell Biol. 22 (2020) 1091–1102, https://doi.org/10.1038/s41556-020-0566-0.
[30] Y. Wang, N. Li, X. Zhang, T. Horng, Mitochondrial metabolism regulates macrophage biology, J. Biol. Chem. 297 (2021) 100904, https://doi.org/10.1016/j.jbc.2021.100904.
[31] Z. S, X. K, D. Ma, Y. Q, X. M, Mussel-inspired alginate gel promoting the osteogenic differentiation of mesenchymal stem cells and anti-infection, Mater. Sci. Eng. C 69 (2016), https://doi.org/10.1016/j.msec.2016.06.044.
[32] Y. Zou, Z. Shan, Z. Han, J. Yang, Y. Lin, Z. Gong, L. Xie, J. Xu, R. Xie, Z. Chen, Z. Chen, Regulating Blood Clot Fibrin Films to Manipulate Biomaterial-Mediated Foreign Body Responses, vol. 6, Research (Wash D C), 2023, p. 225, https://doi.org/10.34133/research.0225.
[33] E.N. Zhang, J.-P. Clément, A. Alameri, A. Ng, T.E. Kennedy, D. Juncker, Mechanically matched silicone brain implants reduce brain foreign body response, Adv. Mater. Technol. 6 (2021) 2000909, https://doi.org/10.1002/admt.202000909.
[34] N. Noskovicova, R. Schuster, S. Van Putten, M. Ezzo, A. Koehler, S. Boo, N. M. Coelho, D. Griggs, P. Ruminski, C.A. McCulloch, B. Hinz, Suppression of the fibrotic encapsulation of silicone implants by inhibiting the mechanical activation of pro-fibrotic TGF-β, Nat. Biomed. Eng. 5 (2021) 1437–1456, https://doi.org/10.1038/s41551-021-00722-z.
[35] B.N. Brown, R. Londono, S. Tottey, L. Zhang, K.A. Kukla, M.T. Wolf, K.A. Daly, J. E. Reing, S.F. Badylak, Macrophage phenotype as a predictor of constructive remodeling following the implantation of biologically derived surgical mesh materials, Acta Biomater. 8 (2012) 978–987, https://doi.org/10.1016/j.actbio.2011.11.031.
[36] M.T. Wolf, C.L. Dearth, C.A. Ranallo, S.T. LoPresti, L.E. Carey, K.A. Daly, B. N. Brown, S.F. Badylak, Macrophage polarization in response to ECM coated polypropylene mesh, Biomaterials 35 (2014) 6838–6849, https://doi.org/10.1016/j.biomaterials.2014.04.115.
[37] T.D. Zaveri, J.S. Lewis, N.V. Dolgova, M.J. Clare-Salzler, B.G. Keselowsky, Integrin-directed modulation of macrophage responses to biomaterials, Biomaterials 35 (2014) 3504–3515, https://doi.org/10.1016/j.biomaterials.2014.01.007.
[38] S. Chen, Y. Yu, S. Xie, D. Liang, W. Shi, S. Chen, G. Li, W. Tang, C. Liu, Q. He, Local H2 release remodels senescence microenvironment for improved repair of injured bone, Nat. Commun. 14 (2023) 7783, https://doi.org/10.1038/s41467-023-43618-z.
[39] A.K. Huber, N. Patel, C.A. Pagani, S. Marini, K.R. Padmanabhan, D.L. Matera, M. Said, C. Hwang, G.C.-Y. Hsu, A.A. Poli, A.L. Strong, N.D. Visser, J.A. Greenstein, R. Nelson, S. Li, M.T. Longaker, Y. Tang, S.J. Weiss, B.M. Baker, A.W. James, B. Levi, Immobilization after injury alters extracellular matrix and stem cell fate, J. Clin. Investig. 130 (2020) 5444–5460, https://doi.org/10.1172/JCI136142.
[40] F.Y. McWhorter, T. Wang, P. Nguyen, T. Chung, W.F. Liu, Modulation of macrophage phenotype by cell shape, Proc. Natl. Acad. Sci. U. S. A. 110 (2013) 17253–17258, https://doi.org/10.1073/pnas.1308887110.
[41] C.B. Forsyth, D.A. Solovjov, T.P. Ugarova, E.F. Plow, Integrin alpha(M)beta(2)-mediated cell migration to fibrinogen and its recognition peptides, J. Exp. Med. 193 (2001) 1123–1133, https://doi.org/10.1084/jem.193.10.1123.
[42] H. Tatsukawa, Y. Furutani, K. Hitomi, S. Kojima, Transglutaminase 2 has opposing roles in the regulation of cellular functions as well as cell growth and death, Cell Death Dis. 7 (2016) e2244, https://doi.org/10.1038/cddis.2016.150.
[43] Z. Yang, X.-W. Zhang, F.-F. Zhuo, T.-T. Liu, Q.-W. Luo, Y.-Z. Zheng, L. Li, H. Yang, Y.-C. Zhang, Y.-H. Wang, D. Liu, P.-F. Tu, K.-W. Zeng, Allosteric activation of transglutaminase 2 via inducing an “open” conformation for osteoblast differentiation, Adv. Sci. 10 (2023) e2206533, https://doi.org/10.1002/advs.202206533.
[44] K.E. Sosnovski, T. Braun, A. Amir, D. Moshel, M. BenShoshan, K.L. VanDussen, N. Levhar, H. Abbas-Egbariya, K. Beider, R. Ben-Yishay, S. Asad Ali, S.R. Moore, S. Kugathasan, I. Abramovich, E. Glick Saar, B. Weiss, I. Barshack, E. Gottlieb, T. Geiger, S. Ben-Horin, I. Ulitsky, J.S. Hyams, L.A. Denson, Y. Haberman, GATA6-AS1 regulates intestinal epithelial mitochondrial functions, and its reduced expression is linked to intestinal inflammation and less favourable disease course in ulcerative colitis, J Crohns Colitis 17 (2023) 960–971, https://doi.org/10.1093/ecco-jcc/jjad006.
[45] R. Sun, H. Li, Y. Chen, M. Hu, J. Wang, Tubuloside A alleviates postmyocardial infarction cardiac fibrosis by inhibiting TGM2: involvement of inflammation and mitochondrial pathway apoptosis, Int. Immunopharmacol. 143 (2024) 113324, https://doi.org/10.1016/j.intimp.2024.113324.
[46] Mitochondrial dysfunction prevents repolarization of inflammatory macrophages, Cell Rep. 17 (2016) 684–696, https://doi.org/10.1016/j.celrep.2016.09.008.
[47] S. Rius-Pérez, I. Torres-Cuevas, I. Millán, Á.L. Ortega, S. Pérez, PGC-1α, inflammation, and oxidative stress: an integrative view in metabolism, Oxid. Med. Cell. Longev. 2020 (2020) 1452696, https://doi.org/10.1155/2020/1452696.
[48] N. Laurens, P. Koolwijk, M.P.M. de Maat, Fibrin structure and wound healing, J. Thromb. Haemostasis 4 (2006) 932–939, https://doi.org/10.1111/j.1538-7836.2006.01861.x.
[49] M.L. Meizlish, Y. Kimura, S.D. Pope, R. Matta, C. Kim, N.H. Philip, L. Meyaard, A. Gonzalez, R. Medzhitov, Mechanosensing regulates tissue repair program in macrophages, Sci. Adv. 10 (2024), https://doi.org/10.1126/sciadv.adk6906 eadk6906.
[50] W. Li, H. Liang, Y. Ao, B. Tang, J. Li, N. Li, J. Wang, Y. Du, Biophysical cues of bone marrow-inspired scaffolds regulate hematopoiesis of hematopoietic stem and progenitor cells, Biomaterials 298 (2023) 122111, https://doi.org/10.1016/j.biomaterials.2023.122111.

[51] S.K. Nair, S. Basu, B. Sen, M.-H. Lin, A.N. Kumar, Y. Yuan, P.J. Cullen, D. Sarkar, Colloidal gels with tunable mechanomorphology regulate endothelial morphogenesis, Sci. Rep. 9 (2019) 1072, https://doi.org/10.1038/s41598-018-37788-w.
[52] T.A. Wynn, K.M. Vannella, Macrophages in tissue repair, regeneration, and fibrosis, Immunity 44 (2016) 450–462, https://doi.org/10.1016/j.immuni.2016.02.015.
[53] P. Heher, S. Mühleder, R. Mittermayr, H. Redl, P. Slezak, Fibrin-based delivery strategies for acute and chronic wound healing, Adv. Drug Deliv. Rev. 129 (2018) 134–147, https://doi.org/10.1016/j.addr.2017.12.007.
[54] A. Saraswathibhatla, D. Indana, O. Chaudhuri, Cell–extracellular matrix mechanotransduction in 3D, Nat. Rev. Mol. Cell Biol. 24 (2023) 495–516, https://doi.org/10.1038/s41580-023-00583-1.
[55] M.J. Flick, X. Du, D.P. Witte, M. Jirousková, D.A. Soloviev, S.J. Busuttil, E.F. Plow, J.L. Degen, Leukocyte engagement of fibrin(ogen) via the integrin receptor alphaMbeta2/Mac-1 is critical for host inflammatory response in vivo, J. Clin. Investig. 113 (2004) 1596–1606, https://doi.org/10.1172/JCI20741.
[56] Z. Yao, Y. Fan, L. Lin, R.E. Kellems, Y. Xia, Tissue transglutaminase: a multifunctional and multisite regulator in health and disease, Physiol. Rev. 104 (2024) 281–325, https://doi.org/10.1152/physrev.00003.2023.
[57] M. Maamra, O.M. Benayad, D. Matthews, C. Kettleborough, J. Atkinson, K. Cain, H. Bon, H. Brand, M. Parkinson, P.F. Watson, T.S. Johnson, Transglutaminase 2: development of therapeutic antibodies reveals four inhibitory epitopes and confirms extracellular function in fibrotic remodelling, Br. J. Pharmacol. 179 (2022) 2697–2712, https://doi.org/10.1111/bph.15774.
[58] S.N.P. Murthy, S. Iismaa, G. Begg, D.M. Freymann, R.M. Graham, L. Lorand, Conserved tryptophan in the core domain of transglutaminase is essential for catalytic activity, Proc. Natl. Acad. Sci. 99 (2002) 2738–2742, https://doi.org/10.1073/pnas.052715799.
[59] S. Eligini, S. Fiorelli, E. Tremoli, S. Colli, Inhibition of transglutaminase 2 reduces efferocytosis in human macrophages: role of CD14 and SR-AI receptors, Nutr. Metabol. Cardiovasc. Dis. 26 (2016) 922–930, https://doi.org/10.1016/j.numecd.2016.05.011.
[60] M. D'Eletto, F. Rossin, L. Occhigrossi, M.G. Farrace, D. Faccenda, R. Desai, S. Marchi, G. Refolo, L. Falasca, M. Antonioli, F. Ciccosanti, G.M. Fimia, P. Pinton, M. Campanella, M. Piacentini, Transglutaminase type 2 regulates ER-mitochondria contact sites by interacting with GRP75, Cell Rep. 25 (2018) 3573–3581.e4, https://doi.org/10.1016/j.celrep.2018.11.094.
[61] W. Zheng, Q. Chen, H. Liu, L. Zeng, Y. Zhou, X. Liu, Y. Bai, J. Zhang, Y. Pan, C. Shao, SDC1-dependent TGM2 determines radiosensitivity in glioblastoma by coordinating EPG5-mediated fusion of autophagosomes with lysosomes, Autophagy 19 (2023) 839–857, https://doi.org/10.1080/15548627.2022.2105562.
[62] F. Rossin, M. D'Eletto, L. Falasca, S. Sepe, S. Cocco, G.M. Fimia, M. Campanella, P. G. Mastroberardino, M.G. Farrace, M. Piacentini, Transglutaminase 2 ablation leads to mitophagy impairment associated with a metabolic shift towards aerobic glycolysis, Cell Death Differ. 22 (2015) 408–418, https://doi.org/10.1038/cdd.2014.106.
[63] Y.-X. Wei, Y.-H. Wang, X.-T. Yu, L.-L. Hu, X.-Q. Luo, S.-C. Sun, Loss of LRRK2 activity induces cytoskeleton defects and oxidative stress during porcine oocyte maturation, Cell Commun. Signal. 23 (2025) 2, https://doi.org/10.1186/s12964-024-01997-w.
[64] S. Phuyal, P. Romani, S. Dupont, H. Farhan, Mechanobiology of organelles: illuminating their roles in mechanosensing and mechanotransduction, Trends Cell Biol. 33 (2023) 1049–1061, https://doi.org/10.1016/j.tcb.2023.05.001.
[65] Y. Ji, Y. Lin, J. He, Y. Xie, W. An, X. Luo, X. Qiao, Z. Li, Research progress of mitochondria and cytoskeleton crosstalk in tumour development, Biochim. Biophys. Acta Rev. Canc 1880 (2024) 189254, https://doi.org/10.1016/j.bbcan.2024.189254.
[66] J. Davis, T. Meyer, M. Smolnig, D.G.J. Smethurst, L. Neuhaus, J. Heyden, F. Broeskamp, E.S.M. Edrich, O. Knittelfelder, D. Kolb, T. von der Haar, C. W. Gourlay, P. Rockenfeller, A dynamic actin cytoskeleton is required to prevent constitutive VDAC-dependent MAPK signalling and aberrant lipid homeostasis, iScience 26 (2023) 107539, https://doi.org/10.1016/j.isci.2023.107539.
[67] A. Pagliuso, T.N. Tham, J.K. Stevens, T. Lagache, R. Persson, A. Salles, J.-C. Olivo-Marin, S. Oddos, A. Spang, P. Cossart, F. Stavru, A role for septin 2 in Drp1-mediated mitochondrial fission, EMBO Rep. 17 (2016) 858–873, https://doi.org/10.15252/embr.201541612.
[68] A.S. Wolberg, Thrombin generation and fibrin clot structure, Blood Rev. 21 (2007) 131–142, https://doi.org/10.1016/j.blre.2006.11.001.
[69] L. Xiao, Y. Ma, R. Crawford, J. Mendhi, Y. Zhang, H. Lu, Q. Zhao, J. Cao, C. Wu, X. Wang, Y. Xiao, The interplay between hemostasis and immune response in biomaterial development for osteogenesis, Mater. Today 54 (2022) 202–224, https://doi.org/10.1016/j.mattod.2022.02.010.